II WORKSHOP DE APLICAÇÕES
DE TÉCNICAS ELETROMAGNÉTICAS
PARA O MONITORAMENTO AMBIENTAL

Effects of interfacial Polarization on Low Frequency Soil Dielectric Permittivity

Prof. Dr Dani Or, LASEP – EPFL, Lausanne - Suiça.

Dani Or – Chair of Soil and Terrestrial Environmental Physics (STEP)
Department of Environmental Sciences (D-UWIS)
Swiss Federal Institute of Technology (ETHZ), Switzerland

Abstract:

The presence of free charges and numerous discontinuities separating liquid, gas, and solid phases in partially-saturated soils give rise to Maxwell-Wagner polarization that may significantly effect bulk dielectric permittivity measurements. The low frequency (<100 MHz) dielectric permittivity response to changes in ambient temperature and salinity is wet soils is complex and must be accounted for with introduction of new water content sensors. . Model calculations based on the Maxwell-Wagner-Brugermann-Hanai (MWBH) theory are supported by direct measurements using a network analyzer, showing an increase in soil bulk dielectric permittivity with increasing temperature and with higher bulk electrical conductivity at low frequency range (<100 MHz). Beyond a certain frequency, the decrease in permittivity of free water becomes dominant and results in a decrease in soil bulk dielectric permittivity with increasing temperature. This crossover frequency can be predicted as a function of solution electrical conductivity (EC) as confirmed in limited tests. The dielectric permittivity inferred from TDR waveform travel time analysis is not significantly influenced by the low frequency range of the dielectric spectrum. In contrast, dielectric permittivity sensors operating at frequencies lower than 100 MHz are likely to show significant sensitivity to factors affecting the Maxwell-Wagner effect (temperature and electrical conductivity), hence requiring special care in measurement interpretation.

1. Introduction

Time Domain Reflectometry (TDR) is now the standard method for repetitive and non-destructive measurement of soil water content [Topp and Ferre, 2002; Robinson et al., 2003]. Key to the success of TDR is the relatively simple and broadly applicable relationships between measured bulk dielectric permittivity and water content, such as the empirical Topp equation [Topp et al., 1980].

$$\theta = 4.3\times10^{-6}\varepsilon_b^3 - 5.5\times10^{-4}\varepsilon_b^2 + 2.92\times10^{-2}\varepsilon_b - 5.3\times10^{-2} \quad \textbf{(1)}$$

Numerous applications of Topp equation have established its usefulness for mineral soils; however, in some cases permittivity is significantly influenced by factors other than soil water content alone resulting in significant deviations from the Topp equation [Dirksen and Dasberg, 1993; Schaap et al., 1996]. Some of the factors affecting permittivity measurements are electrical conductivity, temperature, soil texture, particle shape, bound water and phase configuration [Friedman and Robinson, 2002; Jones and Or, 2002; Robinson et al., 2003; Robinson et al., 2005; Miyamoto et al., 2005]. Figure 1 illustrates variations in complex dielectric spectrum of liquids and other mixtures vary

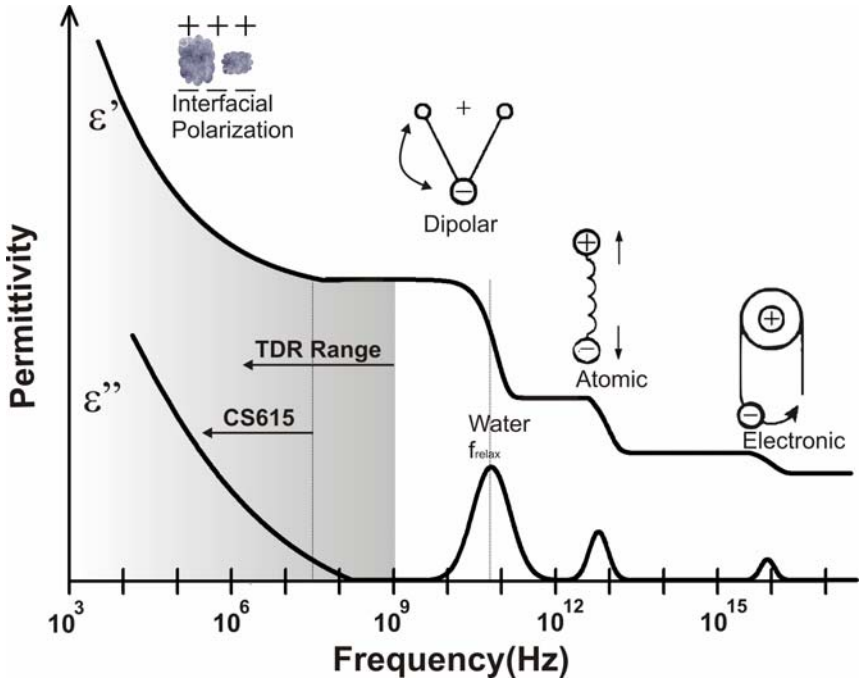

Figure 1: Schematic of the dielectric permittivity spectrum and various relaxation processes occurring at different frequencies (soil water content approximate measurement ranges of TDR and CS615 are indicated by arrows).

with frequency due to different relaxation processes. Most electromagnetic methods and sensors used for soil water content measurement operate at frequencies ranging from kHz to GHz in which interfacial polarization also known as the Maxwell-Wagner (M-W) effect) plays an important role.

The M-W effect occurs in mixtures composed of segregated constituents with different dielectric permittivity and electrical conductivity. Soils represent mixtures of constituents with considerably different electrical properties (liquids, solids, air) separated by numerous interfaces (as shown in Figure 2). For an external electrical field applied across a soil mixture, the normal component of the electrical field must be equal across interfaces

separating constituents with different dielectric properties. This requirement results in charge accumulation or interfacial charging often accompanied by considerable enhancement of bulk dielectric permittivity (to values that are higher than the sum of its components) [Alvarez, 1973; Chelidze and Gueguen, 1999; West et al., 2003]. Interfacial processes remain active in the frequency range of kHz to MHz, well within the range of measurement of many soil water content sensors including TDR. The extent of M-W

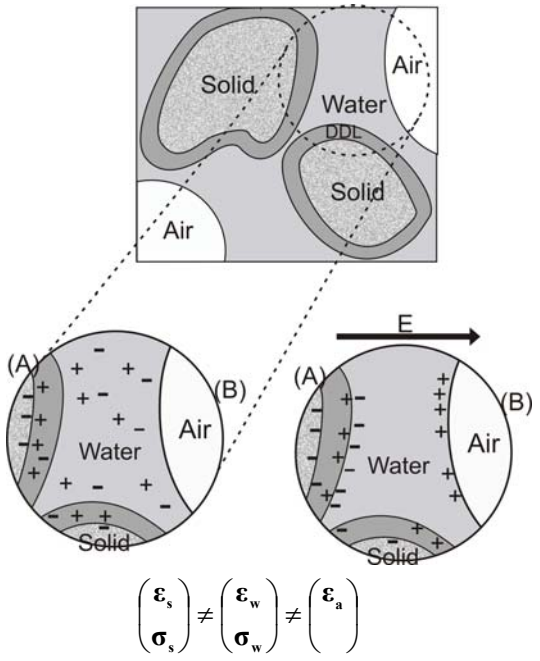

Figure 2: Interfacial polarization (M-W effect) in soil due to perturbation of ionic charges; (A) alignment of charges associated with solid-liquid-air interface by applied electrical field; and (B) accumulation of charges at the solid-liquid-air interface due to mismatch in electrical conductivity between the phases

effect on measured dielectric permittivity is strongly affected by soil electrical conductivity and ambient temperature.

The primary objective of this study was to quantify the contribution of the M-W effect to soil bulk dielectric permittivity measured by TDR and other dielectric-based sensors. Our interest was motivated by the need to interpret bulk dielectric permittivity measurements and reconcile water content measurements from different sensors often operating at low frequency, where the M-W effect is dominant. Additionally, near-surface dielectric measurements of soil water content often exhibit distinct temperature effects [Halbertsma et al., 1995; Wraith and Or, 1999]. These thermal effects are attributed either to reduction in dielectric permittivity of free water with increasing temperature, or the release of bound water with increasing temperature [Or and Wraith, 1999] resulting in conflicting trends in bulk permittivity response. The thermal sensitivity of the M-W effect offers an additional mechanism for thermal effects on dielectric determination of water content that must be considered. For this study, we have chosen to focus on these effects on the popular TDR method; however, we offer general insights applicable to other sensors. We address these questions using a general modeling framework capable of incorporating effects of M-W polarization on dielectric permittivity under a wide range of soil textures and water contents, and considering various ambient temperatures and electrical conductivities.

2. Theoretical Considerations

2.1 MWBH and the Differential Effective Medium Approximation (DEMA)

The Differential Effective Medium Approximation (DEMA) has been used to simulate bulk permittivity of porous earth materials. It incorporates effects of geometrical arrangement of various phases in the microstructures of porous media, and the effect of electrical conductivity of the aqueous phase. Details of DEMA and alternative models are described in Sen et al., [1981]; Norris, [1985]; Endres and Redman, [1996]; Asami, [2002]; Cosenza et al., [2003], and in the context of the modeling reported here, by Chen and Or [2006a].

The effective permittivity according to DEMA approach is based on the following iterative steps: 1) a component of the mixture is selected as the background to which

other components are added as inclusions; 2) adding infinitesimal volumes of inclusions of the other phases (with prescribed configuration) into the background matrix; 3) performing a homogenization of the new mixture; 4) using the homogenized mixture as initial background for the next step of inclusion addition; 5) repeat these steps until the the target volume fraction of phases/inclusion has been reached (see details in Chen and Or [2006a]).

For present modeling, we employ a simplified three-phase DEMA model for spherical inclusions (Eq. 2) to calculate influences of electrical conductivity, temperature, and the M-W polarization on bulk permittivity and on TDR waveforms. The high degree

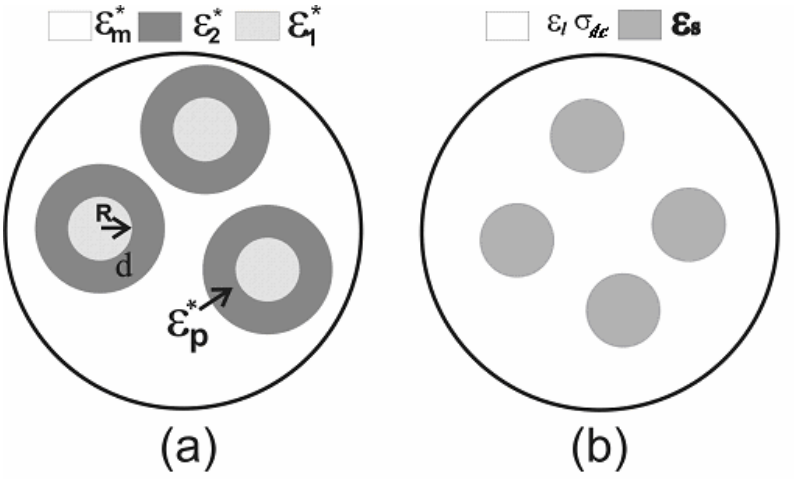

Figure 3: (a) Definition sketch of spherical inclusion coated by a shell used for MWBH's DEMA three-phase system; (b) Wagner's two-phase model with low concentration inclusion.

of saturation in most of the soil samples tested in this study simplifies our considerations to the SWA configuration only (discussion of other phase configurations is given in Chen and Or [2006a]).

$$\left(\frac{\varepsilon^* - \varepsilon_p^*}{\varepsilon_m^* - \varepsilon_p^*}\right)\left(\frac{\varepsilon_m^*}{\varepsilon^*}\right)^{1/3} = 1-\phi$$

$$\varepsilon_p^* = \varepsilon_2^* \frac{2(1-\lambda)\varepsilon_2^* + (1+2\lambda)\varepsilon_1^*}{(2+\lambda)\varepsilon_2^* + (1-\lambda)\varepsilon_1^*} \qquad (2)$$

$$\lambda = \left(\frac{R}{R+d}\right)^3$$

Where ε_m^* and ε_p^* are the complex dielectric permittivity of selected background matrix and the adding inclusion, which is a core material covered by a shell of another material, *d* is the thickness of the shell, *R* is the radius of the core, ε_1^* and ε_2^* are the complex permittivities of the core and shell respectively (Fig. 2a).

2.2 Effects of Fluid Phase Configuration

Partial saturation is associated with complex configuration of liquid and gaseous phases in media pore space which play an important role in measured dielectric permittivity of the mixture [Sen, 1981; Chelidze and Gueguen, 1999; Cosenza et al., 2003]. Phase configuration and geometry define the types of interactions and shape of an electrical field across phase discontinuities. In the context of the proposed MWBH-DEMA model of coated inclusions, phase configuration is equivalent to defining a particular integration path for incremental phase addition to the mixture [Cosenza et al., 2003]. At a given water content and porosity whether we consider an air-water-solid (AWS) configuration (air entrapped in a water shell inclusions [bubbles] embedded in a background of solid matrix), or solid-water-air (SWA) where solid grains coated with water are placed in a background of air result in considerably different bulk permittivity, even with same types of constituents and volume fractions (see Figure 4). For coated spheres, Friedman [1998] considered all possible combinations of the three phases and reduced these into a smaller subset based on physical arguments (e.g., affinity of water to attach onto hydrophilic solid surfaces) and symmetry considerations. Friedman [1998] eliminated candidate configurations based on their deviation from Topp's [1980] model. In this study we adhered to hydrophilic interactions between solid and water and considered configurations with SW or WS combinations. Additionally, considering the broad spectrum of porous media and measurement frequencies examined here, the two end member configuration chosen were: AWS for dielectric behavior at the low saturation range, and SWA close to saturation. We observed that the concave and steep rise in effective permittivity at the low saturation in the data of Knight and Nur [1987, e.g. their Fig. 10] and others can be represented only by relationships corresponding to AWS configuration , whereas SWA configuration captures the convex and steep increase in measured permittivity at high saturations (e.g., Fig. 4). These configurations can also

be viewed as preferred sequences of phase mixing rather than reflection of physical configurations.

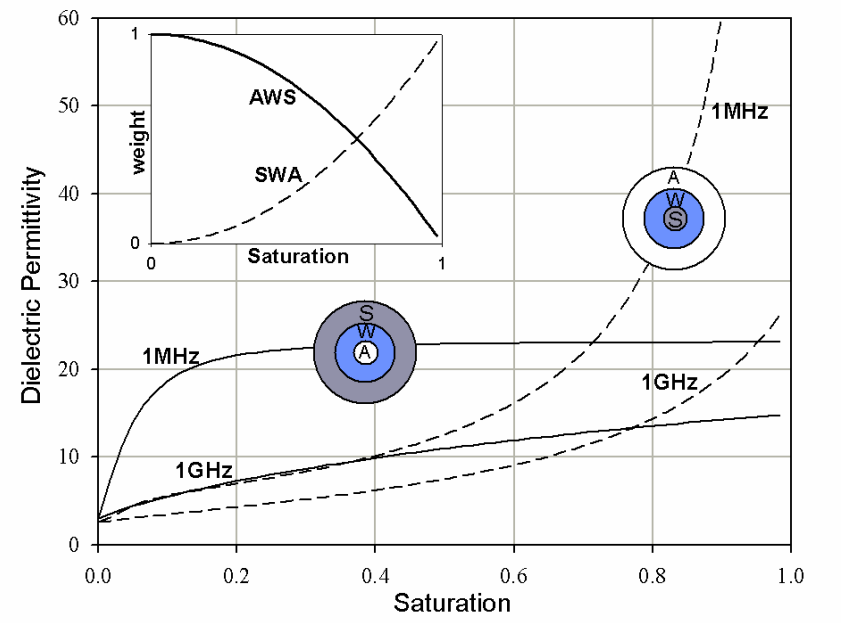

Figure 4: Dielectric Permittivity vs. saturation degree for a hypothetical mixture composed of AWS and SWA phase configurations at frequency of 1MHz and 1GHz (porosity= 40%, and aqueous solution electrical conductivity 0.1S/m). Solid lines for simulated permittivity by AWS phase configuration at 1MHz and 1GHz. Dashed lines are simulated permittivity by SWA phase configuration at 1MHz and 1GHz).

Additionally, the volume fractions of each of the two configurations at different saturations are unknown. Roth [1990], Friedman [1998], Cosenza et al. [2003] and others have proposed the use of degree of saturation (S) as a potential physically-based weight function that naturally signifies transition from one phase configuration to the other. Friedman [1998] compared models of different phase configurations with Topp's equation and proposed a linear combination of two end-member phase configurations weighted by saturation degree S. In our tests of this approach, we found that the weight function (or volume fraction) providing best fit for all data set was $\alpha=S^2$:

$$\varepsilon_{eff} = (1-\alpha) * \varepsilon_{AWS} + \alpha * \varepsilon_{SWA} \qquad (3)$$
$$\alpha = S^2$$

We evaluated more rigorous methods for combining contributions of different phase configurations to effective permittivity by considering an additional DEMA step,

and simple EMA and Maxwell-Garnett mixing models discussed by Friedman [1998] and others.

The DEMA step for combination of AWS and SWA two phase configurations is given by:

$$\left(\frac{\varepsilon_{eff}-\varepsilon_{AWS}}{\varepsilon_{SWA}-\varepsilon_{AWS}}\right)\left(\frac{\varepsilon_{AWS}}{\varepsilon_{eff}}\right)^{1/3}=\alpha \qquad \textbf{(4)}$$

$$\alpha = S^2$$

The EMA formulation of two phases (configurations) according to Sen [1981] is:

$$\varepsilon_{eff} = \left\{\frac{\left[(1-\alpha)(\varepsilon_{SWA}-2\varepsilon_{AWS})+\alpha(\varepsilon_{AWS}-2\varepsilon_{SWA})\right]^2}{16}+\frac{\varepsilon_{AWS}\varepsilon_{SWA}}{2}\right\}^{1/2} - \frac{\left[(1-\alpha)(\varepsilon_{SWA}-2\varepsilon_{AWS})+\alpha(\varepsilon_{AWS}-2\varepsilon_{SWS})\right]}{4} \qquad \textbf{(5)}$$

$$\alpha = S^2$$

The Maxwell-Garnett model for connecting AWS and SWA phase configurations is [Friedman, 1987]:

$$\varepsilon_{eff} = \varepsilon_{SWA}+3(1-\alpha)\varepsilon_{SWA}\left(\frac{\varepsilon_{AWS}-\varepsilon_{SWA}}{\varepsilon_{AWS}+2\varepsilon_{SWA}-(1-\alpha)(\varepsilon_{AWS}-\varepsilon_{SWA})}\right) \qquad \textbf{(6)}$$

$$\alpha = S^2$$

We evaluated these four different mixing models for a wide range of experimental data. The use of $\alpha=S^2$ was found to be superior to $\alpha=S$ for all models tested, in particular for the simple linear weight function (eq. 3).

2.3 Effects of Maxwell-Wagner Polarization on TDR Waveforms

Detailed description of the TDR method including in-depth discussions concerning waveform analyses are provided in a recent review by Robinson et al [2003]. Here, we provide a concise introduction of the method focusing on key aspects related to incorporation of the M-W effect and impact on measured waveforms essential for water content determination. Typically we measure the propagation velocity of a step voltage signal (with a bandwidth 20kHz to 1.5 GHz for standard equipment such as the Tektronix 1502 cable tester) traveling through a waveguide (TDR probe) embedded in the porous medium. The signal travel time is a function of the permittivity of the material through

which it travels. Signal travel time is inferred from a waveform recorded by the TDR marking the location (time) of the entry and reflection from the end of the probe.

It is instructive to divide the elements giving rise to measured TDR waveform into three parts: the *input signal*, the *system function* (probe geometry and material), and *output signal or waveform* (Fig. 5) [Heimovaara et al., 1994; Friel and Or, 1999]. It is convenient to consider the step signal generated by the instrument after traveling in the coaxial cable connected to the probe as "input signal" (assuming minimal losses in the coaxial cable [Feng, 1999]). The system function reflects the complex interactions between the input signal probe geometry and the electrical properties of the surrounding material. The output signal or measured waveform contains information on travel time along the TDR probe as well as other influences such as attenuation due to charge migration (proportional to bulk electrical conductivity) [Topp and Reynolds, 1998; Jones et al., 2002].

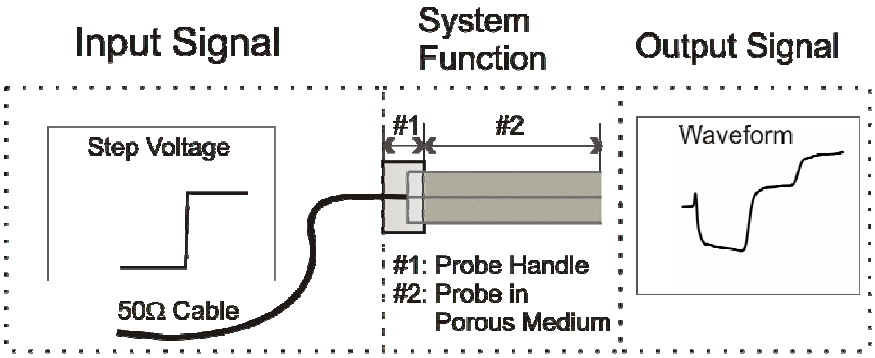

Figure 5: The illustration of TDR input signal, system function, and output signal.

For a linear time-invariant system, the output signal or the reflection waveform r(t) is given by the following convolution integral:

$$r(t) = \int_{-\infty}^{\infty} v_0(t-\tau)s(\tau)d(\tau) \qquad \textbf{(7)}$$

where $v_0(t)$ is the input signal generated by the TDR; s(t) is the system function, which is dependent on the dielectric properties of the material tested (see details in Chen and Or [2006b]); r(t) is the reflection waveform. Conversion of these time-dependent functions into the frequency domain (using the Fast Fourier Transform [FFT] technique)

greatly simplifies the complex convolution integral into a simple multiplication in the frequency domain as follows:

$$R(f) = V_0(f) \bullet S(f) \qquad \textbf{(8)}$$

where R(f), V_0(f) and S(f) are the transformed waveform input signal, and system function in the frequency domain, respectively [Friel and Or, 1999; Lin, 2003; Heimovaara et al., 2004].

S(f) is an explicit function of the complex dielectric permittivity of the porous medium surrounding a TDR probe, hence providing a means for analyzing the effects of M-W polarization on TDR waveforms. This is accomplished in the following steps:

Step1: Calculation of the bulk dielectric permittivity spectrum of the wet porous medium based on the MWBH model (Eq. 2). Followed by calculation of S(f) from the simulated permittivity spectrum;

Step 2: Establishing input signal v_0(t) characteristic of the TDR cable tester from either direct measurements, or from a parametric mode). The input signal v_0(t) is then converted to its frequency domain form V_0(f) using FFT;

Step 3: Multiplying V_0(f) and S(f) as shown in Eq. 8 (the frequency domain equivalent to a convolution integral in the time domain) to obtain the frequency domain representation of the TDR waveform R(f);

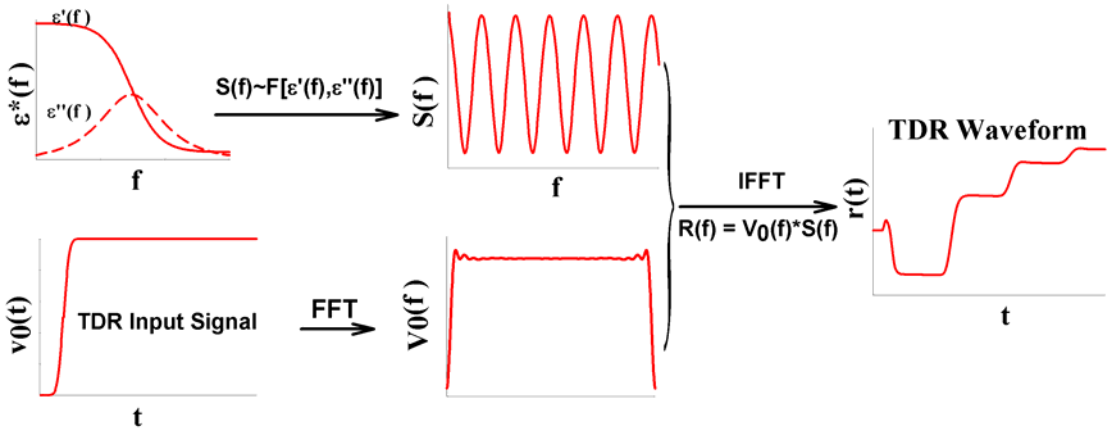

Figure 6: A schematic flowchart for TDR waveform simulation using complex permittivity, system function and FFT/IFFT techniques.

Step 4: Transforming the reflection signal waveform R(f) back to the time domain (using inverse FFT) to obtain the simulated TDR waveform r(t) which is then compared

with measured-TDR waveform to assess the impact of the M-W effect on travel time analyses. A schematic flowchart is depicted in Figure 6, detailed calculations are provided in Chen and Or [2006b].

3. Applications and Dielectric Permittivity Determination Using TDR

3.1 Dielectric Permittivity of Low and High Clay Content Porous Media

Campbell [1990] has used a network analyzer and a coaxial sample holder to measure the dielectric permittivity of partially saturated Wilder silt soil (porosity=0.41) reported at frequencies of 1MHz, 5MHz and 50MHz. A constant electrical conductivity value of 0.05 S/m for the soil solution was assumed for all calculations. The soil bulk permittivity was modeled using two phase configurations, AWS and SWA weighed by saturation squared as weight function, and combined by four different schemes summarized by equations 3 to 6.

Model calculations using different approaches to combining effective permittivities of end-member phase configurations were evaluated with measured data sets. A sample comparison for Campbell's [1990] Wilder silt soil measurements is depicted in Fig. 5 (a and b) illustrating the generally superior performance of the Maxwell-Garnet (M-G) scheme (equation 8) with a single weight $\alpha=S^2$ providing best fit to most data evaluated. Linear combination (equation 3) provided better match than DEMA and EMA schemes, consequently, we retained the M-G and linear combination of phase configurations for subsequent evaluation of modeling results.

Results depicted in Fig. 7 show a sharp increase in dielectric permittivity with the introduction of small amounts of water into the dry soil (<5% water content) for both 1MHz and 5MHz frequencies. A rapid increase of dielectric permittivity at low water-contents is characteristic of AWS phase configuration (Fig. 4).

Based on measurements of Knight and Nur [1987] and analyses in Chen and Or [2006a] we conclude that dielectric measurements in porous media with low clay-content show a sharp rise of dielectric permittivity at low water-content at low measurement frequency. The magnitude of the rise decreases with increasing measurement frequency.

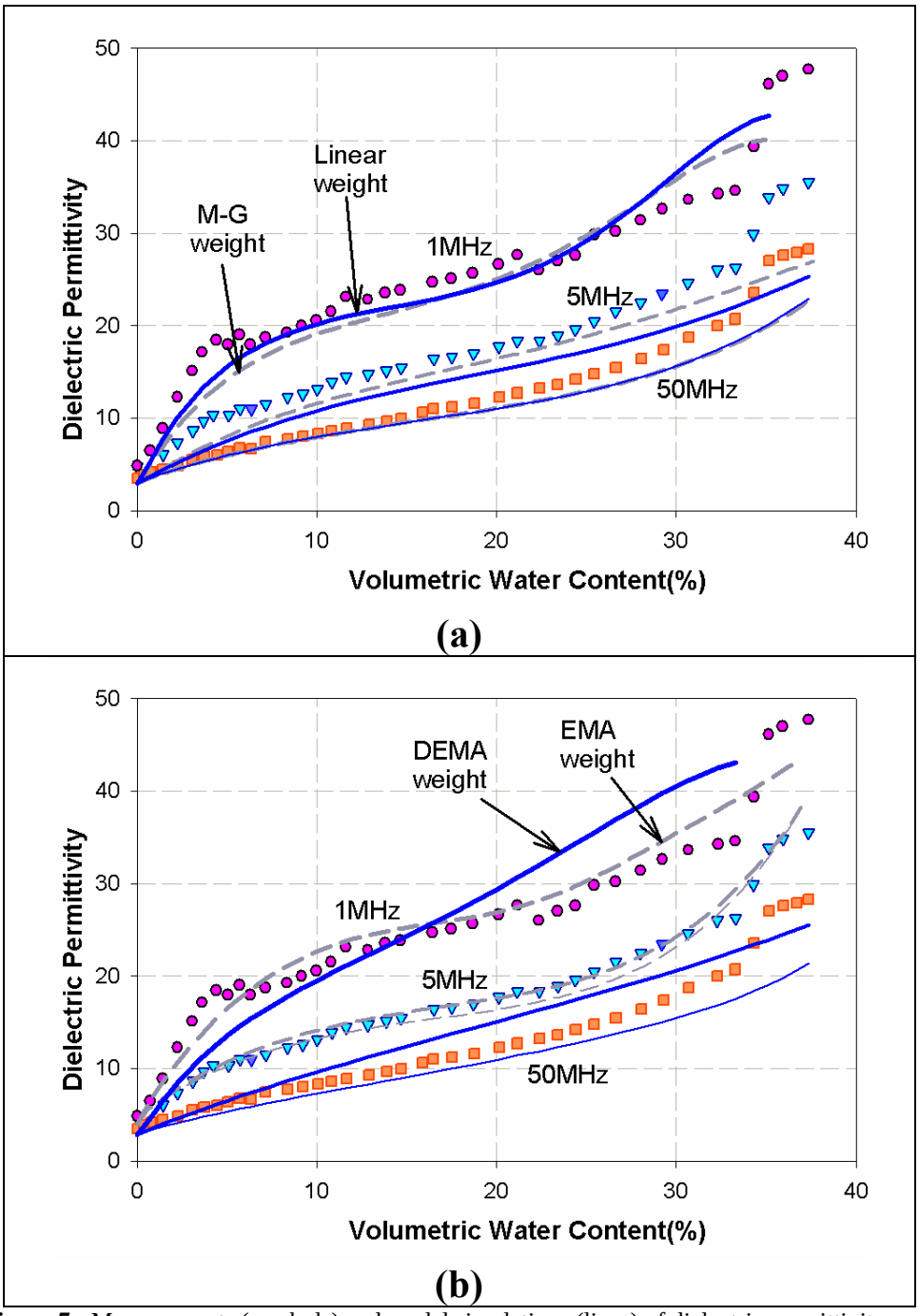

Figure 7: Measurements (symbols) and model simulations (lines) of dielectric permittivity vs. volumetric water content for Wilder Silt soil [Campbell, 1990]. (a) Solid lines are simulated permittivity by linear weight of AWS and SWA phase configurations (equation 3); dashed lines are the simulated permittivity by Maxwell-Garnett (M-G) weight function (equation 6); (b) Solid lines are simulated permittivity by DEMA scheme (equation 4); dashed lines represent simulated permittivity by EMA scheme (equation 5).

The best match with our modeling approach is obtained with AWS as the dominant phase configuration at low saturation. This could be explained by wetting patterns of low porosity sandy soils and sandstones occurring by association with solid surfaces and

crevices first without complete expulsion of air (incomplete pore filling) followed by gradual filling of large pores at higher saturations.

For soils with high clay content we consider Saarenketo [1998] who measured the dielectric behavior of Houston Black clay and Beaumont clay. The porosity of Houston Black clay is assumed 0.6, and solution electrical conductivity is 1.5 S/m [Cosenza et al, 2003]. Model results were in very good agreement with measured values (Fig. 6 lines). Similar results were obtained for Beaumont clay (porosity=0.6 and solution electrical conductivity of 0.8 S/m [Cosenza et al., 2003]) using ellipsoidal inclusions (not shown). All simulations consider AWS and SWA phase configurations weighted with by saturation degree using equations 3 and 6.

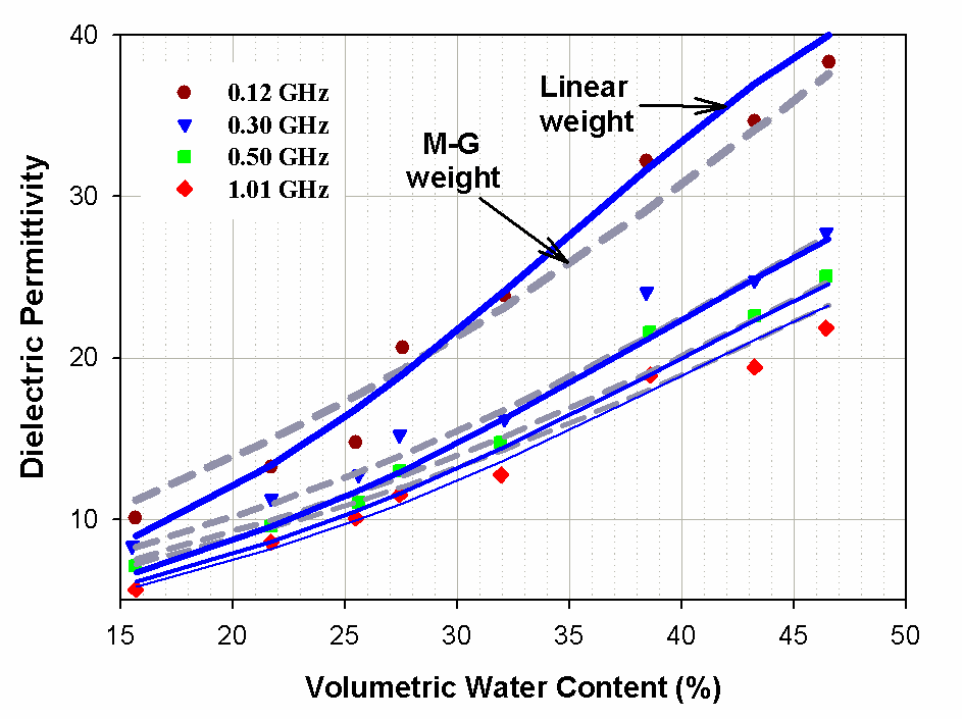

Figure 8: Measured (symbols) and simulated (lines) dielectric permittivity vs. volumetric water content at four frequencies based on Houston Black clay data reported by Saarenketo [1998]. Solid lines represent simulated permittivity by linear weight function; dashed lines for simulated permittivity by Maxwell-Garnett (M-G) weight function.

The proposed model and phase configuration weight function resulted in good agreement with dielectric measurements of soils with appreciable clay content at different measurement frequencies. The nonlinear response of dielectric permittivity behavior at higher water contents is attributed to dominance of SWA phase configuration.

3.2 Measured and Simulated TDR Waveforms and Dielectric Spectra

To test the procedure outlined in the previous section we used a Network Analyzer (N-A) (Agilent 8753D equipped with High Temperature Dielectric Probe [Agilent 85070E]) to obtain direct measurement of the dielectric spectrum of soils or known liquids. TDR waveforms where obtained from a Tektronix 1502C connected to a computer. Following tests using water and ethanol reported in the appendix, we conducted tests using Woodbridge sandy loam nearly saturated with 0.125 S/m aqueous solution. The median particle size was 0.085mm, and the porosity was 0.44 (nearly saturated water content ~ 0.41m^3/m^3). The steps outlined previously were followed in simulating the dielectric spectrum using the simplified version of the MWBH model Eq. 2 (line Fig. 9a). The modeled spectrum was used in the calculation of the system response function in the frequency domain which was then used to simulate the TDR waveform (line Fig. 9b). The measured permittivity from N-A was 22.0 (the average of the spectrum's flat region near 1GHz). The measured permittivity from TDR waveform travel time analysis was 21.4. The resulting permittivity was relatively insensitive to frequencies in the range between100MHz and1GHz (simulated permittivity near 100MHz ~ 21.0, and from simulated TDR waveform ~20.6).

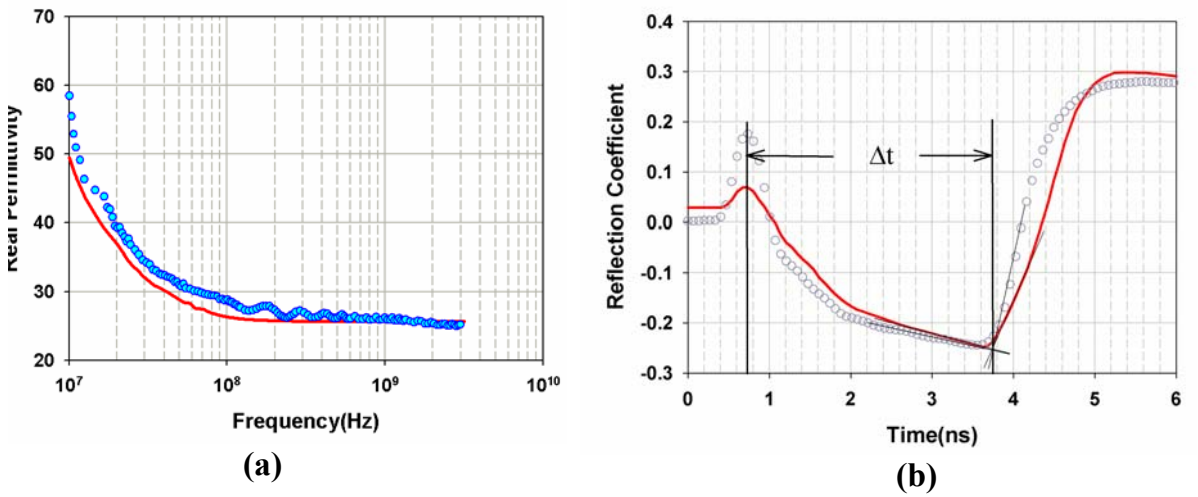

Figure 9: Comparison between measurements and simulations in Woodbridge sandy loam (around 0.44 porosity and 0.41water content). (a) Simulated spectrum (solid line) using MWBH model vs. Measured data (symbols) from N-A; (b) Simulated waveform (solid line) based on spectrum simulation in (a) vs. TDR-measured Waveform (symbols).

The results in Fig. 9 show good agreement between simulated and measured values both in the time and frequency domains, inspiring confidence in the method for simulation of waveforms in soils. These preliminary results also indicate that TDR waveform analysis is influenced by dielectric permittivity values corresponding to frequencies higher than 100 MHz (past the M-W relaxation). This important aspect will be tested in subsequent sections for different electrical conductivities and ambient temperatures using a similar modeling approach.

3.3 The Maxwell-Wagner Effect on Dielectric Permittivity and TDR Waveforms

3.3.1 Effects of the Maxwell-Wagner Polarization on Dielectric Permittivity

The soil minerals are often treated as electrical insulators (non-conductive materials) and electrical conductivity is associated with properties of the soil aqueous phase. An increase is the aqueous phase electrical conductivity (EC) tend to enhance the M-W effect on bulk permittivity of the soil mixture and its frequency dependency. The EC of the soil aqueous phase was the input parameter used in our model, and it is distinguished from soil bulk electrical conductivity.

Illustration of the relationships between electrical conductivity and frequency-dependent permittivity for the MWBH model (Eq. 2) is complicated by the 1/3 power and integrations. Instead we demonstrate these dependencies using the simpler model of Wagner for dilute inclusion concentration (Fig. 3b) considering hypothetical two-phase mixture [Sherman, 1968]. Assuming a mixture with solid inclusions that are perfect insulators (zero electrical conductivity) and ε_s permittivity, embedded in a background liquid with σ_{dc} electrical conductivity and ε_l permittivity (Fig. 3b), the frequency dependent permittivity of this mixture is explicitly given by:

$$\varepsilon^* = \varepsilon_l \frac{2(1-\phi_s)\varepsilon_l + (1+2\phi_s)\varepsilon_s}{(2+\phi_s)\varepsilon_l + (1-\phi_s)\varepsilon_s} + \frac{\Delta\varepsilon}{1+j\omega\tau} + \frac{\sigma^*}{j\omega\varepsilon_0} \qquad (9)$$

where

$$\Delta\varepsilon = \frac{9\phi_s(1-\phi_s)\varepsilon_s^2}{(2+\phi_s)^2\left[2\varepsilon_l + \varepsilon_s + \phi_s(\varepsilon_l - \varepsilon_s)\right]} \qquad (10)$$

$$\tau = \frac{1}{2\pi f_r}, \qquad f_r = \frac{(2+\phi_s)}{2\pi\varepsilon_0\left[2\varepsilon_l + \varepsilon_s + \phi_s(\varepsilon_l - \varepsilon_s)\right]}\sigma_{dc} \qquad (\mathbf{11})$$

$$\sigma^* = \frac{2(1-\phi_s)}{(2+\phi_s)}\sigma_{dc} \qquad (\mathbf{12})$$

where ε_0 is the dielectric permittivity of free space (8.8541×10^{-12} farad/m), ϕ_s is the volumetric fraction of the solid inclusions. ω is the angular frequency ($\omega=2\pi f$), $j=\sqrt{-1}$, τ is the relaxation time, and f_r is the M-W relaxation frequency. Eq. 9 clearly demonstrates the dependency of bulk dielectric permittivity on relaxation frequency, which, in turn, is dependent on background solution electrical conductivity σ_{dc} (Eq. 11). Similar relationships exist for the MWBH model [Hanai and Sekine, 1986] albeit the mathematical representation is more complicated.

To examine the effect of different electrical conductivities, we conducted two sets of experiments measuring TDR waveforms and N-A spectra simultaneously. For the first set we used Ottawa sand (assumed spherical shape, average particle size of 0.11mm, estimated porosity is around 0.38) nearly saturated with de-ionized (DI) water and 0.54 S/m aqueous solution (water content for these two samples ~ $0.34 m^3/m^3$). Modeling and measurement results are depicted in Fig. 10 showing differences in the spectra for the two values of EC in the low frequency range (less than 100MHz) (symbols in Fig. 10a for N-A measurements). In contrast, the dielectric permittivity at frequencies higher than 100MHz was practically identical well beyond 1GHz (in Fig. 10a, N-A measured permittivity for DI water at 1GHz is 22.25 and for 0.54S/m solution is 22.30). Based on these input parameters, we calculated the frequency dependent dielectric permittivity spectrum using the MWBH model (Eq. 2). Simulated real part of the dielectric spectrum was in good agreement with experimental data (Fig. 10a, solid lines). Simulated permittivity values were close to corresponding measured values, about 22.8 for frequencies higher than 100 MHz for both solutions.

For the second set of experiments we used Woodbridge sandy loam nearly saturated with DI water, 0.11 S/m and 0.52 S/m aqueous solutions (porosity is around 0.44, water content is $0.41 m^3/m^3$ for the three samples). The N-A measured real permittivities of the Woodbridge sandy loam saturated with DI water, 0.11 S/m and 0.52 S/m solutions were 24.11, 23.76 and 23.78, respectively (see symbols in Fig. 10b). The simulated

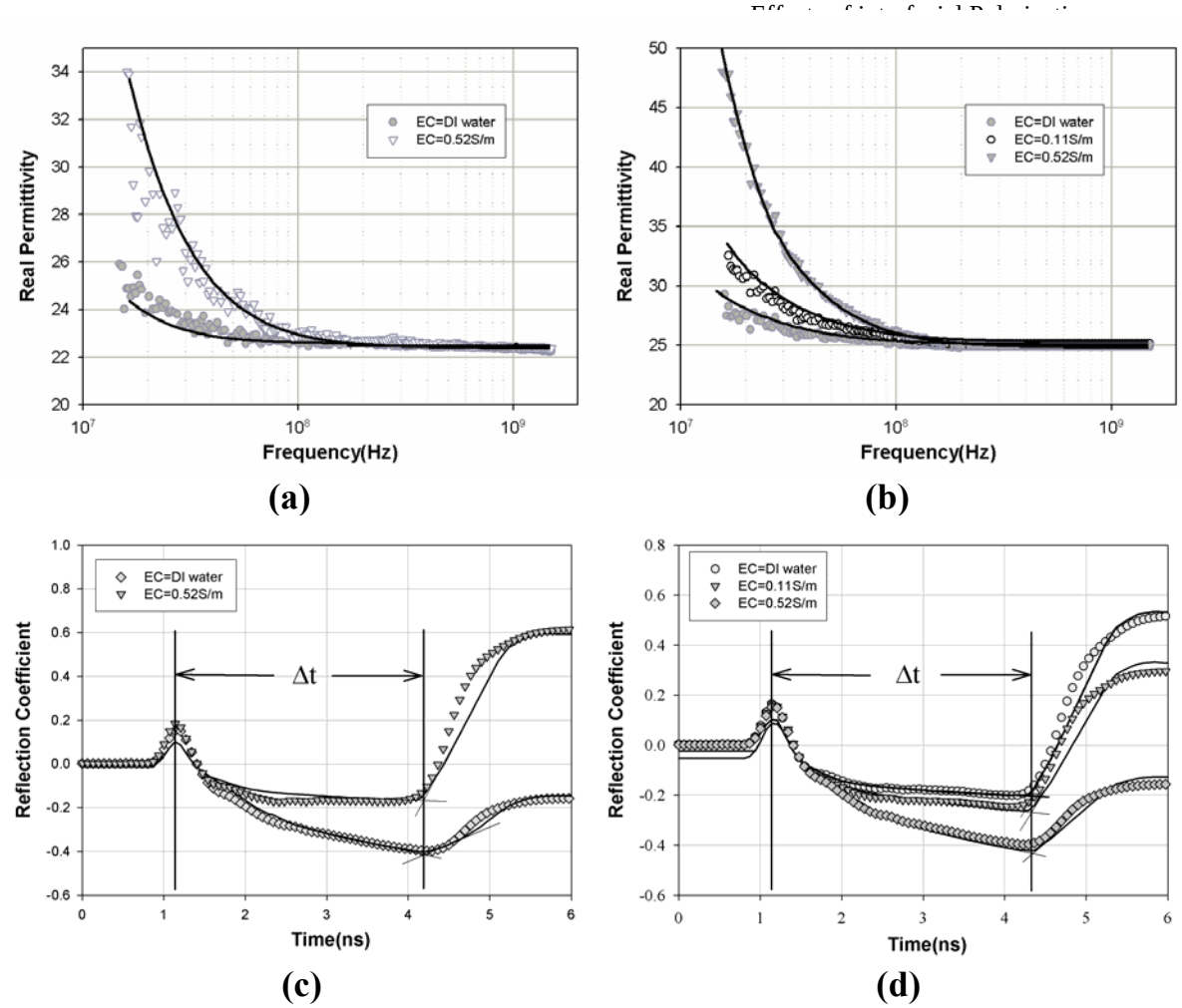

Figure 10: (a) Measured (symbols) and simulated (lines) dielectric spectra for Ottawa sand saturated with DI water and 0.54S/m aqueous solution (porosity ~38%; volumetric water content ~34%). (b) Measured (symbols) and simulated (lines) dielectric spectra for Woodbridge sandy loam saturated with three aqueous solutions (DI water, 0.11 and 0.52 S/m solution) of different electrical conductivities (porosity ~44%; water content ~41%). (c) The corresponding simulated waveforms (lines) compared with measured TDR waveforms (symbols) for Ottawa sand. (d) The corresponding simulated TDR waveforms (symbols), in media of different electrical conductivity, compared with measured TDR waveform (lines) for Woodbridge sandy loam.

permittivity spectra depicted in Fig. 10b (lines) show reasonable agreement with measurements and converge to similar value of dielectric permittivity ~25.9 above 100 MHz for the three samples. Significant differences in dielectric permittivity are exhibited at the low frequency range (<100MHz) for the different saturating solution EC. Increasing EC results in higher dielectric permittivity at a given (low) frequency value and shifts the curve (and relaxation) to higher frequency.

These effects could influence bulk dielectric permittivity measurements in porous media with similar water content but different electrical conductivities. Moreover, considering the ubiquity of free ionic charges in soils and formation of numerous

additional gas-air interfaces in unsaturated soils could enhance the impact of M-W polarization on dielectric permittivity measurements with sensors operating at relatively low frequencies from KHz to 100MHz. The results also suggest that in the high frequency range (>100MHz), the electrical conductivity's influence on the real part of the dielectric permittivity spectrum is negligible.

3.3.2 Effects of the Maxwell-Wagner Polarization on TDR Waveforms

Next we examine the impact of EC and changes in the dielectric spectrum on TDR waveforms and travel time analyses. The evaluation proceeds by comparison between measured and simulated waveforms (using dielectric spectrum from MWBH model). The comparisons between measured (symbols) and simulated (lines) TDR waveforms in saturated Ottawa sand and Woodbridge SL are shown in Figs. 10c and 10d. Resulting permittivity values from travel time analyses of these waveforms are summarized in Table 1.

Table 1. Comparison of dielectric permittivity values deduced from measured and simulated TDR waveforms (using travel time analyses) for two porous media saturated with different aqueous solutions

	Soil Solution	**Dielectric permittivity**	
		Measurement	***Simulation***
Ottawa sand	DI Water	22.68	22.35
	0.54 S/m	22.13	22.35
Woodbridge sandy loam	DI Water	23.71	24.82
	0.11S/m	23.24	24.82
	0.52 S/m	23.47	24.82

The results show practically no effect of EC on TDR-measured dielectric permittivity in these saturated porous samples. Despite significant differences in the dielectric spectra associated with different saturating solution EC (Figs. 10a and 10b) at the low frequency, the resulting travel times were practically unaffected (yielding similar dielectric permittivity values for all EC levels – Table 1). The shape of TDR waveforms exhibit significant effect of EC through attenuation and rounding of reflected signal, however,

reflection locations determined by tangent line analyses [Wraith and Or, 1999; Robinson et al., 2003] occurred at the same location on the waveform for all EC values. Based on the results presented we conclude that features used for travel time analyses of TDR waveforms are dominated by permittivity values at the high frequency range (>100MHz) suggesting that M-W effect may not play an important role in TDR measurements.

3.4 Temperature Effects on Permittivity and TDR Waveforms

3.4.1 The Role of Temperature in the M-W Effect and Dielectric Permittivity

Near-surface water content measurements are subject to diurnal and seasonal variations in soil temperature. Here we consider variations in the range from 5°C to 55°C. Typically, the permittivity of solid soil particles and air is not greatly affected in this temperature range, whereas soil water permittivity and electrical conductivity show much greater thermal sensitivity. The dielectric permittivity of free water and solution EC vary with temperature as follows [Stogryn, 1971; Weast, 1986]:

$$\varepsilon_w^{'}(T) = 87.74 - 0.4008T + 9.398\times10^{-4}T^2 - 1.410\times10^{-6}T^3 \qquad \textbf{(13)}$$

$$\sigma_{dc}(T) = \sigma_{dc(25^o)} \exp[-\Delta(2.033\times10^{-2} + 1.266\times10^{-4}\Delta + 2.464\times10^{-6}\Delta^2)] \qquad \textbf{(14)}$$

where T is in °C, $\Delta = (25 - T)$, $\varepsilon_w^{'}$ is the relative permittivity of soil water, and σ_{dc} is the electrical conductivity of soil water. These relationships show a decrease in soil water permittivity with increasing temperature (hence a potential for decreasing bulk permittivity of the soil mixture). However, the electrical conductivity increases with temperature (enhanced ion mobility) thereby enhancing M-W effect, which, in turn, could increase soil bulk dielectric permittivity at low frequency while shifting the range of M-W effect to higher frequencies. For a 1°C increase, σ_{dc} gains about 2% and $\varepsilon_w^{'}$ is reduced by 0.3%.

These two competing processes were considered in the framework of the MWBH model [Hanai and Sekine, 1986]. The temperature dependencies (Eqs. 13 and 14) were incorporated into the calculations for a hypothetical porous medium (porosity of 0.4) "saturated" (volumetric water content of 0.35 m^3/m^3 to mimic experimental conditions) with aqueous solution of EC=0.05 S/m. Calculated dielectric spectra of the hypothetical porous medium at the temperatures range of 5°C to 55°C are shown in Fig. 11a.

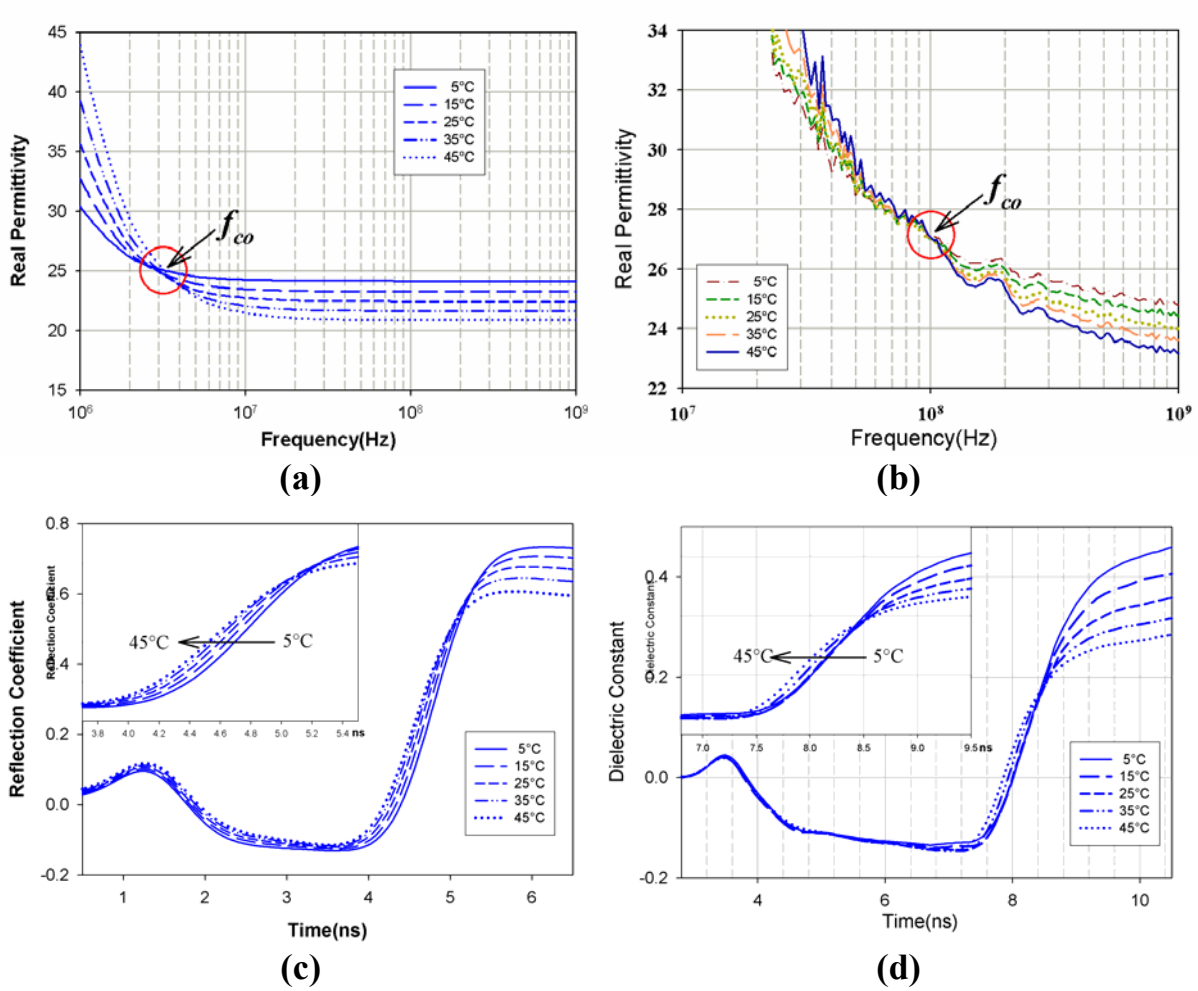

Figure 11: (a) Relative dielectric permittivity vs. frequency at different temperatures (simulated by simplified spherical three-phase system; porosity is 0.4; volumetric water content is 0.35; the porous medium is assumed to be mixed with 0.05S/m water solution). (b) Network Analyzer measured real part of the dielectric permittivity spectrum of Woodbridge SL (water content 0.15 m^3/m^3 and solution EC 0.9 S/m) at different temperatures exhibiting crossover frequency. (c) Corresponding simulated waveform of hypothetical porous medium at different temperatures. (d) Measured TDR waveforms in Woodbridge SL at temperatures and water content corresponding to N-A measurements in (b) above.

The results show existence of a crossover frequency (f_{CO}), below which the dielectric permittivity increases with temperature, and above which the permittivity decreases with increasing temperature. The crossover frequency reflects a range in the bulk permittivity spectrum where the increasing permittivity due to M-W effect of the mixture is balanced by the decrease in dielectric permittivity of free water.

The thermal effect was studied using Woodbridge sandy loam wetted with 0.9S/m solution to water content of 0.15m^3/m^3. The wet soil was allowed to equilibrate and brought to different temperatures using a temperature bath (allowing 24 hours for thermal equilibration). Network analyzer (N-A) measurements of real part of dielectric

permittivity spectrum of the soil confirmed model predictions as seen in Fig. 11b with crossover frequency near 90 MHz.

Further, we conducted series of experiments using Woodbridge sandy loam saturated with different water solutions (EC=0.105S/m, 1.146S/m, 1.389S/m, 1.551S/m, and 1.873S/m), saturated Millville silt loam (EC=0.0846S/m, 0.225S/m, 0.403S/m, 0.682S/m, 0.8S/m, and 0.915S/m), and also Ottawa sand, Kidman sand, and unsaturated Millville silt loam with different solutions. For these measurements, we also corrected for electrode polarization. Chen and Or [2006b] have shown that electrode polarization becomes negligible at frequencies higher than ~20MHz. The measurement results show different crossover frequencies corresponding to different solutions ECs (Fig. 12).

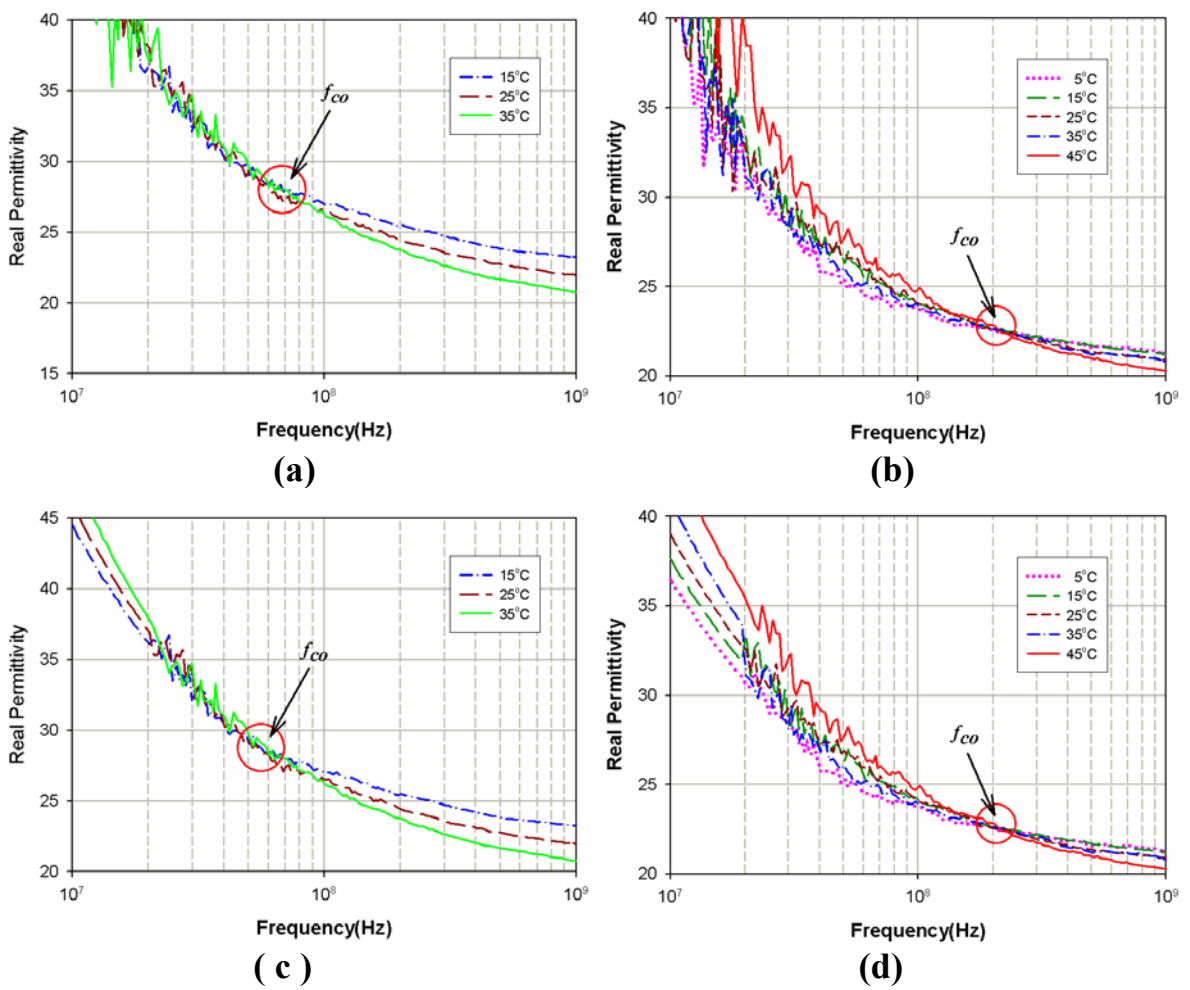

Figure 12: Network analyzer measured dielectric permittivity spectra of two soils subjected to different temperatures (measured at thermal equilibrium). (a) Millville silt loam saturated with 0.682 S/m solution. (b) Woodbridge sandy loam saturated with 1.551 S/m solution. (c) Spectrum of Millville silt loam saturated with 0.682S/m solution after correcting electrode polarization less than 20MHz. (d) Spectrum of Woodbridge sandy loam saturated with 1.551 S/m solution after correcting electrode polarization less than 20MHz.

The opposing trends in thermal effects on free water dielectric permittivity vs. impact on M-W polarization may result in a complex response in soil bulk dielectric permittivity as a function of temperature and frequency. To describe the onset and value of the crossover frequency as a function of key parameters such as solution EC and temperature, we seek an analytical expression using the simplified Wagner's model.

The crossover frequency (f_{CO}) defines a frequency value (or a narrow range) below which the bulk dielectric permittivity increases with temperature increase, and above which the dielectric permittivity decreases as temperature increases. Mathematically, the crossover frequency is defined as the frequency where the derivative of permittivity with respect to temperature equals zero ($\partial\varepsilon/\partial T=0$). Introduction of the thermal dependencies (Eqs. 13 and 14) into Eq. 9, and taking the partial derivatives with respect to temperature, and equating to zero yields the following closed-form expression for the crossover frequency as a function of key input parameters for two-phase mixtures (e.g., soil saturated with saline solution):

$$f_{CO} = \sqrt{\frac{-B+\sqrt{B^2-4AC}}{2A} - f_{M-W}^2} \qquad \textbf{(15)}$$

where

$$-B = \frac{9\phi_l(1-\phi_l)\varepsilon_s^2\sigma_{dc}\left[-(1-\phi_l)(\phi_l+3)\sigma_{dc}\frac{\partial\varepsilon_l}{\partial T} - 2D\frac{\partial\sigma_{dc}}{\partial T}\right]}{(2\pi\varepsilon_0)^2 D^4}$$

$$A = \frac{9\phi_l\varepsilon_s^2}{D}, \qquad D = (2+\phi_l)\varepsilon_s + (1-\phi_l)\varepsilon_l$$

$$C = -2\frac{9\phi_l(1-\phi_l)\varepsilon_s^2\sigma_{dc}^3\left[(1-\phi_l)D\frac{\partial\sigma_{dc}}{\partial T} - (1-\phi_l)^2\sigma_{dc}\frac{\partial\varepsilon_l}{\partial T}\right]}{(2\pi\varepsilon_0)^4 D^6}$$

$$\frac{\partial\varepsilon_l}{\partial T} = -0.4008 + 1.88\times10^{-3}T - 4.23\times10^{-6}T^2 \qquad \textbf{(16)}$$

$$\frac{\partial\sigma_{dc}}{\partial T} = \sigma_{dc(25^o)}\exp[-\Delta(2.033\times10^{-2} + 1.266\times10^{-4}\Delta + 2.464\times10^{-6}\Delta^2)]$$
$$*(2.033\times10^{-2} - 2.532\times10^{-4}\Delta - 7.392\times10^{-6}\Delta^2)$$

$$f_{M-W} = \frac{(1-\phi_l)\sigma_{dc}}{2\pi\varepsilon_0[(2+\phi_l)\varepsilon_s + (1-\phi_l)\varepsilon_l]}$$

The resulting expression for f_{CO} (Eq. 15) is a strong function of solution EC as shown in Fig. 13 (line) for a hypothetical two phase mixture (i.e., saturated soil) with solids volume fraction of ϕ_s = 55% (or ϕ_l = 0.45), and solid permittivity ε_s = 4.6. We conducted a series of tests of this approximation using different soil samples (Millville silt loam, Woodbridge sandy loam, Kidman sand, Ottawa sand, and sand) saturated with a broad range of solution EC (NaCl aqueous solutions). The samples were brought to thermal equilibrium using a temperature controlled water bath and were measured with a network analyzer to obtain their dielectric permittivity spectra. Compilation of these experimental results and visual interpretation of f_{CO} from spectra of a sample under different temperature (similar to results in Fig. 12) provide a general agreement with trends predicted by the model (Eq. 15) even for a few unsaturated (3 phase) samples as seen results (symbols) depicted in Fig. 13. The resulting experimental cross over frequency (f_{CO}) tends to level off at frequencies around 100 MHz for a wide range of solution EC values.

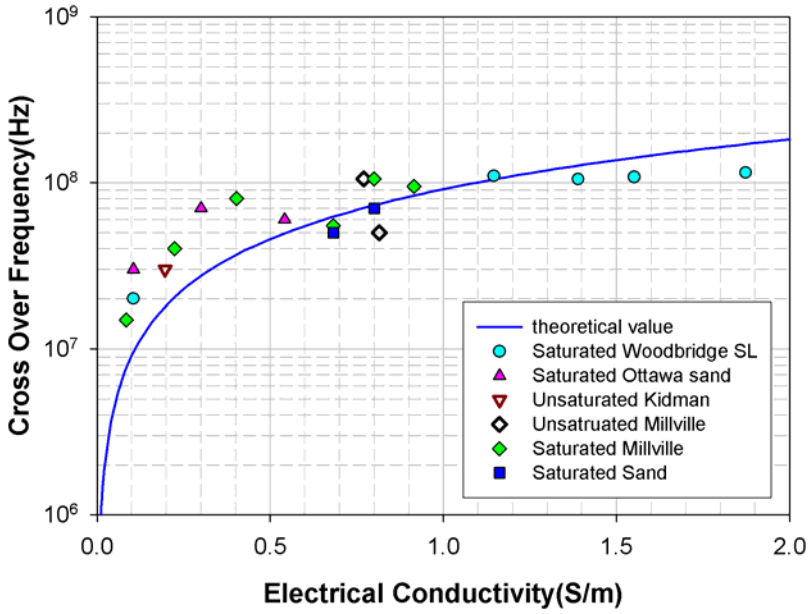

Figure 13: Crossover frequency as a function of solution electrical conductivity in a hypothetical two phase mixture (line). Symbols represent experimental results inferred from N-A measurements at different temperatures similar to those depicted in Fig. 9 (for Millville silt loam, Woodbridge sandy loam, Kidman sand, Ottawa sand, and sand).

The analyses and measurements demonstrate a well-defined low-frequency range in which the M-W effect dominates the behavior of frequency-dependent bulk dielectric permittivity, and a cross-over range where high frequency behavior sets in. The high frequency range is characterized by decreasing permittivity with increasing temperature and convergence of the dielectric permittivity to a nearly constant value (virtually no frequency dependency). For simplicity, we do not consider other thermal effects that might take place at the high frequency range such as release of bound water with increasing temperature [Or and Wraith, 1999], which should affect both N-A and TDR measurements. The value of critical frequency which separates the low- and high-frequency behaviors varies primarily with solution electrical conductivity (there is a weak dependency on water content not explicitly accounted for in the two-phase model). Based on these results we would expect that the thermal response of water content sensors operating at the low frequency range (<100MHz) would probably exhibit an increase in dielectric permittivity with increasing temperature due to the M-W effect. Conversely, sensors operating at the high frequency (>100MHz) would show a decrease in dielectric permittivity with increasing temperature, especially in soils with coarse texture and low surface area where bound water effects are minimal.

3.4.2 Effects of Temperature and M-W Polarization on TDR Measurements

To analyze the combined thermal and M-W polarization effects on TDR waveforms, we employ the procedure outlined in section 2.3 to simulate TDR waveforms for a hypothetical porous medium considering different temperatures. The simulated waveforms (Fig. 11c) are based on the corresponding dielectric permittivity spectra shown in Fig. 11a. Although dielectric permittivity spectra exhibited different trends with increasing temperature, the effect of temperature manifested in simulated TDR waveforms shows only a decrease in travel time with increasing temperature (noting that signal attenuation was affected). This suggests that TDR waveform features used for travel time analyses (i.e., locations of reflections) are determined primarily by high frequency components of the dielectric spectrum (>100MHz). Similar results were obtained for Woodbridge sandy loam comparing N-A measured spectra at different temperatures (Fig. 11b) and the corresponding measured TDR waveforms (Fig. 11d)

showing shorter travel time with increasing temperature. In other words, both simulated and measured TDR waveforms show that while attenuation increases with increasing temperature (effective EC increases), the signal travel time decreases with increasing temperature, confirming the dominance of the high frequency behavior on TDR waveforms.

Summarizing, the thermal response of complex bulk permittivity is influenced by the interplay between effects of EC and temperature on enhancing the M-W effect at the low frequency range, and reducing dielectric permittivity at higher frequency (due to effect on free water permittivity). These factors affect travel time analyses deduced from TDR waveforms at frequencies higher than the crossover frequency (>100 MHz) despite the inherently broad frequency content of TDR signals (20 KHz to 1GHz).

3.5 Effects of Maxwell-Wagner Polarization on Other Dielectric-Based Sensors

The foregoing discussion suggests that sensor measurement frequency is a critical factor in interpretation of dielectric measurements and conversion to water contents, particularly at low frequencies. To illustrate this aspect we use Campbell's [1990] dielectric measurements in soils of different textures obtained at frequencies of 1MHz, 5MHz and 50MHz using a network analyzer and coaxial sample holder. For the fine textured soils (silts and clay soils) measured dielectric permittivity exhibited substantial differences between the various frequencies. For example, Campbell's [1990] measurements (symbols) for Wilder silt soil obtained at two frequencies are depicted in Fig.14. This example illustrates that a volumetric water content of 0.20 m^3/m^3 would correspond to a dielectric permittivity value of ~25 for 1 MHz and to only ~12 at 50 MHz! Alternatively, a measured dielectric permittivity value of 20 with a sensor operating at 1 MHz would correspond to volumetric water content of $0.10 m^3/m^3$ whereas for a sensor operating at 50 MHz this value would correspond to $0.33 m^3/m^3$.

These differences highlight the need for a model that is capable of accounting for low frequency behavior (the M-W effect) and for providing a physically-based link between dielectric permittivity and water content for a given sensor frequency. We used the MWBH model to simulate the dielectric permittivity at different frequencies (Fig. 14, lines, using a combination of AWS and SWA phase configurations as described in Chen

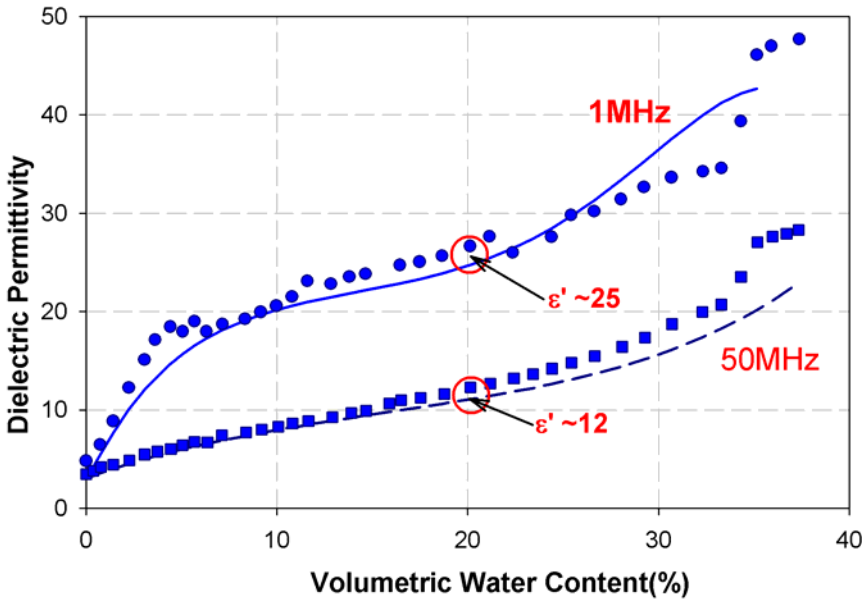

Figure 14: Measured (symbols) and simulated (lines) soil bulk permittivity values of Wilder silt soil as function of volumetric water content at two measurement frequencies of 1 and 50 MHz [Campbell, 1990].

and Or [2006a]). Despite limitations of the modeling results, the simulated lines capture the main trends exhibited by measurements and account for the M-W effect. Results from numerous N-A measurements conducted in our lab using different soil types and EC conditions (not reported) show typical dispersive spectra associated with the M-W effect at frequencies up to ~100MHz (e.g., Figs. 10a and 10b) within which many new dielectric sensors operate. In addition to large changes in frequency-dependent relationships between dielectric permittivity and water content at low frequencies (Fig. 14), field applications are further complicated by thermal sensitivity discussed above, often requiring site specific calibration [Chandler et al., 2004] and are subject to ongoing debate [Nadler, 2005].

4. Summary and Conclusions

The main focus of this study was on the role of the M-W effect associated with inhomogeneous mixtures of constituents with different dielectric properties on bulk dielectric permittivity measurements. A framework based on the MWBH formalism was used to model frequency-dependent dielectric permittivity of soils subjected to different

ambient temperatures and containing aqueous solutions with different values of electrical conductivity. We have used the MWBH model to predict complex permittivity of a three-phase porous medium composed of coated spherical and ellipsoidal inclusions. The model explicitly accounts for the roles of phase configuration, inclusion shape, electrical conductivity (EC), and frequency where the Maxwell-Wagner polarization affects mixture dielectric permittivity.

Modeling results and interpretation of data reported in the literature show the dominant roles of phase configuration and interfacial processes affecting the dielectric permittivity spectrum of wet soils especially at frequencies below 100 MHz. This dependency highlights limitations of standard measurement interpretation based on Topp's equation. Experimental results and physical considerations enable reduction of the number of phase configurations to AWS and SWA configurations only. Moreover, the use of a single saturation-based weight function with simple M-G or linear combination of phase configurations provided a good match with measured permittivity across many soils types, saturation degrees, and frequencies. Results show that particle or inclusion shapes become important for clayey soils especially at lower frequencies.

Through the effects on frequency-dependent dielectric permittivity, we were able to examine the role of the M-W effect on TDR waveforms. The results showed that despite significant effect of M-W polarization on dielectric permittivity at lower frequencies, the effect on travel time analyses of TDR waveforms was negligible. The primary variable affecting the magnitude and frequency of occurrence of the M-W effect within a dielectric permittivity spectrum is the solution electrical conductivity as illustrated analytically and experimentally using network analyzer measurements (Figs. 10a and 10b). However, the effect of EC on TDR waveforms was limited to signal attenuation, with little impact on travel time analyses used to deduce bulk dielectric permittivity and water content (Figs. 10c and 10d).

Analyses of thermal effects on M-W polarization yielded an interesting interplay between amplification of the M-W effect with increasing temperature at low frequency, and monotonic decrease in dielectric permittivity of free water dominating the mixture at higher frequencies. Theoretical predictions were supported by network analyzer measurements of soil dielectric spectra for different temperatures, confirming the

existence of a crossover frequency that separates these two trends. We used Wagner's two-phase dielectric mixing model to develop a closed-form expression for the crossover frequency (Eq. 15). Tests using soil samples saturated with solutions of different EC resulted in reasonable agreement with model prediction of crossover frequency (Fig. 13). The existence of a predictable crossover frequency offers a convenient and physically-based criterion for separating between the low- and high- frequency measurement ranges with respect to dielectric measurements of soil water content.

The negligible impact of the M-W effect on TDR travel time analyses suggests that the effective TDR frequency range is higher than 100MHz, and highlight the need for frequency dependent calibration for interpretation of dielectric measurements using water content dielectric sensors operating at the low frequency range.

Acknowledgements

Funding provided by USDA-NRI under grants 2001-35107-11009 is gratefully acknowledged. The manuscript is based on research conducted at UConn by Yongping Chen during her graduate studies – her dedication and enthusiasm are gratefully acknowledged. The author thanks Jon Wraith and Paolo Castiglione (Montana State Univ.) and David Robinson (Utah State Univ.) for providing soil samples, reviewing of early drafts of this manuscript, and for making many useful suggestions.

References

Alvarez, R. (1973), Complex dielectric permittivity in rocks: a method for its measurement and analysis, *Geophysics*, 38, 920-940.

Asami, K. (2002), Characterization of heterogeneous systems by dielectric spectroscopy, *Progress in Polymer Science.*, 27, 1617-1659.

Bordi, F., C. Cametti, and T. Gili (2001), Reduction of the contribution of electrode polarization effects in the radiowave dielectric measurements of highly conductive biological cell suspensions, *Bioelectrochemisty*, 54, 53-61.

Campbell, J. E. (1990), Dielectric properties and influence of conductivity in soils at one to fifty megahertz, *Soil Sci. Soc. Am. J.*, 54, 332-341.

Chandler, D.G., M. Seyfried, M. Murdock, and J.P. McNamara (2004), Field calibration of water content reflectometers. *Soil Sci. Soc. Am. J.* 68:1501–1507.

Chelidze, T.L., and Y. Gueguen (1999), Electrical spectroscopy of porous rocks: a review-I. Theoretical models, *Geophysics*, 137, 1-15.

Chen, Y. and D. Or. (2006a), Geometrical factors and interfacial processes affecting complex dielectric permittivity of partially saturated porous media. Water Resour. Res , 42, W06423, doi:10.1029/2005WR004744.

Chen, Y. and D. Or (2006b), Effects of Maxwell-Wagner polarization on soil complex dielectric permittivity under variable temperature and electrical conductivity. Water Resour. Res., 42, W06424, doi:10.1029/2005WR004590

Cosenza, P., C. Camerlynck and A. Tabbagh (2003), Differential effective medium schemes for investigating the relationship between high frequency relative dielectric permittivity and water content of soils, *Water. Resour. Res.,* 39, 1-13.

Dirksen, C., and S. Dasberg (1993), Improved calibration of time domain reflectometry soil water measurements, *Soil Sci. Soc. Am. J.*, 57, 660-667.

Endres, A. L. and J.D. Redman (1996), Modeling the electrical properties of porous rocks and soils containing immiscible contaminants, *J Environ. Eng. Geophys.,* 0, 105-112.

Friel, R., and D. Or (1999), Frequency analysis of time-domain reflectometry (TDR) with application to dielectric spectroscopy of soil constituents, *Geophysics*, 64, 707-718.

Friedman, S.P., and D. A. Robinson (2002), Particle shape characterization using angle of repose measurements for predicting the effective permittivity and electrical conductivity of saturated granular media, *Water. Resour. Res*., 38, 1236, doi:10.1029/2001WR000746.

Halbertsma, J., E. van den Elsen, H. Bohl, and W. Skierucha (1994), Temperature effects on TDR determined soil water content, in *Proceedings of the Symposium: Time-Domain Reflectometry Applications in Soil Science, Research Center Foulum, Sep. 16, 1994*, edited by L.W. Petersen and O.H. Jacobsen, SP Rep. 11(3), pp. 35-37, Danish Inst. Of Plant and Soil Sci., Lyngby, Denmark, 1995.

Hanai, T., and K. Sekine (1986), Theory of dielectric relaxation due to the interfacial polarization for two-component suspension of spheres, *Colloid & Pollymer Sci.*, 264, 888-895.

Heimovaara, T.J. (1994), Frequency domain analysis of time domain reflectometry waveforms 1. Measurements of the complex dielectric permittivity of soils, *Water. Resour. Res*., 30, 189-199.

Heimovaara, T.J., J.A. Huisman, J.A. Vrugt, and W. Bouten (2004), Obtaining the spatial distribution of water content along a TDR probe using the SCEM-UA bayesian inverse modeling scheme, *Vadose Zone J.*, 3, 1128-1145.

Jones, S.B. and D. Or (2002), Surface area, geometrical and configuration effects on permittivity of porous media, *J. Non-Crystalline Solids*, 305, 247-254.

Jones, S.B., J.M. Wraith, and D. Or (2002), Time Domain Reflectometry (TDR) measurement principles and applications, *Hydrological Processes*, 16, 141-153.

Jones, S.B. and D. Or (2004), Frequency domain analysis for extending time domain reflectometry water content measurement in highly saline soils, *Soil Sci. Soc. Am. J.*, 68, 1568-1577.

Knight, R. J. and A. Nur (1987), The dielectric constant of sandstones, 60 KHz to 4MHz, Geophysics, 52, 644-654.

Lin, C.P. (2003), Analysis of nonuniform and dispersive time domain reflectometry measurement systems with application to the dielectric spectroscopy of soils, *Water. Resour. Res*., 39, 1012-1023.

Liu, S.H. (1985), Fractal model for the ac response of a rough interface, *Phys. Rev. Lett.*, 55, 529-532.

Macdonald, J.R. (Ed.) (1987), Impedance spectroscopy, Wiley, New York.

Miyamoto, T., T. Annaka and J. Chikushi (2005), Extended dual composite sphere model for determining dielectric permittivity of andisols, *Soil Sci. Soc. Am. J.*, 69, 23-29.

Nadler, A. (2005), Comments on "Field calibration of water content reflectometers", *Soil Sci. Soc. Am. J.*, 69, 1356-1357.

Norris, A. N. (1985), A differential scheme for the effective moduli of composites, *Mech. Mater.*, 4, 1-16.

Or, D., and J.M. Wraith (1999), Temperature effects on soil bulk dielectric permittivity measured by time domain reflectometry: A physical model, *Water. Resour. Res*., 35, 371-383.

Robinson, D. A., S. B. Jones, J. M. Wraith, D. Or, and S. P. Friedman (2003), A Review of advances in dielectric and electrical conductivity measurement in soils using time domain reflectometry, *Vadose Zone J.*, 2, 444-475.

Robinson, D.A., M.G. Schaap, D. Or, S.B. Jones (2005), On the effective measurement frequency of time domain reflectometry in dispersive and nonconductive dielectric materials, *Water. Resour. Res*., 41, W02007, doi:10.1029/2004WR003816.

Roldán-Toro, R. and J.D. Solier (2004), Wide-frequency-range dielectric response of polystyrene latex dispersions, *J. Coll. Int. Sci.*, 274, 76-88.

Saarenketo, T. (1998), Electrical properties of water in clay and silty soils, J. Appli. Geophys., 40, 73-88.

Schaap, M., L. de Lange, and T.J. Heimovaara (1996), TDR calibration of organic forest floor media, *Soil Technol.*, 11, 205–217.

Sen, P.N., C. Scala and M.H. Cohen (1981), A self-similar model for sedimentary rocks with application to the dielectric constant of fused glass beads, *Geophysics,* 46, 781-795.

Sherman, P. (1968), *Emulsion science,* Academic Press, London.

Stogryn, A. (1971), Equations for calculating the dielectric constant of saline water, *IEEE Trans. Microwav. Theory Techn.*, MIT19, 733-736.

Stuchly, M.A. and S.S. Stuchly (1980), Coaxial line reflection methods for measuring dielectric properties of biological substances at ratio and microwave frequencies – A review, *IEEE Trans. Instrum. Meas.*, IM-29, 176-183.

Topp, G.C., J.L. Davis, and A.P. Annan (1980), Electromagnetic determination of soil water content: Measurements in coaxial transmission lines, *Water. Resour. Res*., 16, 574-582.

Topp, G.C. and W.D. Reynolds (1998), Time domain reflectometry: a seminal technique for measuring mass and energy in soil, *Soil & Tillage Research*, 47, 125-132.

Topp, G. C., and P. A. Ferre (2002), Water content, in Methods of Soil Analysis Part 4 – Physical Methods, edited by J.H. Dane and G..

Weast, R.C. (1986), CRC Handbook of Chemistry and Physics, 67th ed., CRC Press, Boca Raton, FL.

West, L.J., K. Handley, Y. Huang, and M. Pokar (2003), Radar frequency dielectric dispersion in sandstone: implications for determination of moisture and clay content, *Water. Resour. Res*., 39, 1026-1037.

Wraith, J.M., and D. Or (1999), Temperature effects on soil bulk dielectric permittivity measured by time domain reflectometry: Experimental evidence and hypothesis development, *Water. Resour. Res*., 35, 361-369.